ROYAL SOCIETY OF CHEMISTRY

PAPER

Check for updates

A nickel(II) complex of a naphthaldehyde-derived bis-imine ligand for sunlight-driven dye remediation: mechanistic, intermediate identification, and recyclability studies

Nilotpal Goswami,[a] Diganta Kumar Bharali,[ab] Nabajit Barman[cd] and Pranjit Barman [ID] *[a]

Dyes have been proven to act as persistent organic pollutants in both freshwater bodies and the marine environment. Thus, suitable dye remediation measures have become obligatory to save aquatic biosystems and maintain human health. This work presents a study on the photocatalytic remediation of cationic dyes using a nickel(II) complex (**NiL₁Et**). The **NiL₁Et** complex was synthesized using the ONS donor ligand (**L₁**) and confirmed using spectroscopic techniques and elemental analysis. The Ni(II) complex **NiL₁Et** adopts a square planar geometry, which was envisioned through a computational study. The experimentally estimated direct band gap of 2.19 eV is in agreement with the HOMO−LUMO energy obtained in the computational study. This establishes the semiconductor-like property of the **NiL₁Et** complex. Moreover, the slower electron−hole recombination rate of the excited complex, as inferred from the emission intensities, further demonstrates the potential of **NiL₁Et** as a photocatalyst. Methylene blue (MB) was used as the model dye, and a maximum degradation efficiency of 80.15% was achieved using **NiL₁Et** within 60 min under natural sunlight and without any artificial light source. The effects of various parameters, including the catalyst amount, dye concentration, reaction time, pH, and H₂O₂ dose, were analyzed. It was observed that the complex could be efficiently used as a photocatalyst for 5 catalytic cycles. Furthermore, insights into the mechanistic pathway of MB degradation were obtained. The path of MB degradation was predicted by determining the intermediate species generated during the degradation process using LC-MS.

Sustainability spotlight

Organic dyes, when released untreated, can pollute water bodies. Although a number of Fe(II)/Fe(III) and Cu(II) Schiff base complexes have been efficient in the degradation of organic pollutants, only a few Ni(II) Schiff base complexes were found to be efficient. This is due to their low degradation efficiency and extended degradation period. The **NiL₁Et** complex was found to be capable of degrading a cationic dye with high efficiency in a short period under natural sunlight, without the requirement of additional light sources. Thus, it is a sustainable and more energy- and cost-effective option. Our work contributes to achieving the Sustainable Development Goals (SDGs) 6 (Clean Water and Sanitation) and 14 (Life Below Water).

1 Introduction

A major concern of humankind is tackling the rising global water scarcity. The indiscriminate pollution of water bodies further limits the availability of safe drinking water. Numerous industry-based goods, including commodities such as pharmaceutical products, cosmetics, paints, and dyes, have been proven to be persistent organic pollutants due to their non-biodegradability.[1]

Organic dyes constitute a class of organic molecules that play a major role in the pollution of water bodies. A large number of dyes are used in substantial quantities across various printing, textile, and rubber industries. The effluents from these industries contain a number of organic dyes, which can be toxic.[2,3] Common wastewater treatment plants in the textile industry are inefficient at completely removing dyes.[2] Thus, the effluents containing these dyes, like methylene blue (MB), when released into water bodies, not only affect the turbidity, pH, temperature, and color of the water but also lead to water pollution, eutrophication, and the production of various perilous by-products,

[a]Department of Chemistry, National Institute of Technology, Silchar, Assam, 788010, India. E-mail: pranjit@che.nits.ac.in; barmanpranjit@yahoo.co.in; Tel: +91-9435374128

[b]Department of Chemistry, Biswanath College, 784176, Assam, India

[c]Advanced Materials Laboratory, Physical Sciences Division, Institute of Advanced Study in Science and Technology, Guwahati, 781035, India

[d]Academy of Scientific and Innovative Research (AcSIR), Ghaziabad, 201002, India

which are generated as a result of these dyes undergoing different chemical reactions.[4] These dyes can persist in the environment for prolonged periods of time and contaminate the groundwater, thereby posing serious health hazards, as they can be highly toxic and carcinogenic.[2] This is why researchers worldwide are devoting significant research attention to the development of sustainable and effective methods for the remediation of dyes like MB from effluents and water sources.

Photocatalytic advanced oxidation processes (AOPs) have emerged as some of the most popular and effective protocols for the remediation of organic dye pollutants. Such processes involve the transfer of electrons from the conduction band into the valence band of the photocatalyst when irradiated with light. When the electrons and holes from the photocatalyst come in contact with H_2O_2, O_2, or H_2O, radical oxygen species (ROS) like $\cdot OH$ and $\cdot O^{2-}$ are produced. The ROS thus produced cause the photodegradation of organic pollutants like dyes.[5]

Various nanoparticles and polymers have been reported to catalyze the photocatalytic degradation of organic pollutants, such as dyes.[5–8] However, metal nanomaterials were found to have specific adverse effects. These mainly include the high cost of synthetic routes and the toxicity of certain metal nanomaterials. Some of them were also found to interact with other species in the reaction medium during the degradation process. Moreover, separating and recycling nanomaterials is a complicated and expensive process that often requires sophisticated instruments. Some serious health hazards have been linked to the usage of various metal-based nanomaterials.[9] Thus, researchers have studied different catalyst species as alternatives to these metal nanomaterials for their potential in achieving higher efficiency with a low-cost synthetic route and substantially lower toxicity.

Various metal complexes have shown great potential as photocatalysts for the mineralization of organic pollutants in aquatic systems. However, these metal complexes have always been associated with low heterogeneity and lower stability in reaction media, which leads to a lower recyclability of the catalytic species. In this regard, certain Schiff base metal complexes have proven to be excellent photocatalysts for the degradation of organic pollutants, including dyes, pharmaceutical products, and other organic molecules. Some Schiff base complexes were found to exhibit high degradation efficiency with desired recyclability over consecutive catalytic cycles.[10] However, a majority of Schiff base metal complexes reported as photocatalysts for the degradation of organic pollutants, such as dyes, are mostly Fe(II)/Fe(III) and Cu(II) complexes.[4,10,11] Very few Ni(II) Schiff base complexes have been reported to be effective photocatalysts for the degradation of organic dyes. Low degradation efficiency and a longer degradation time were major drawbacks for most of the few reported Ni(II) Schiff base complexes.[12–14] However, very few Ni(II) Schiff base complexes were also capable of achieving degradation efficiencies greater than 90%.[15,16] This inspired us to study the photocatalytic capability of Ni(II) complexes of highly conjugated Schiff base ligands. A lower HOMO–LUMO energy gap is expected in such complexes in the presence of a conjugated ligand, thereby facilitating charge separation when irradiated with light. This, in turn, will favour higher photocatalytic activity.

In this work, we present the development of a complex (**NiL₁Et**) consisting of a Ni(II) centre being ligated to a naphthaldehyde-derived unsymmetric Schiff base-based ONS donor ligand (**L₁**). The **NiL₁Et** complex was evaluated for its photocatalytic efficiency in the degradation of MB dye *via* an advanced oxidation process under sunlight.

2 Experimental

2.1. Chemicals and instruments

All the required chemicals and solvents were procured from BLDpharm, SRL, and Merck India Ltd.

The vibrational spectra were obtained using a Bruker 3000 Hyperion Microscope FT-IR spectrometer. A 400-MHz JEOL JNM ECS400 NMR spectrometer was employed to record the ^1H NMR spectra. ESI-mass and LC-MS spectra were obtained using a XEVO G2-XS QTOF mass spectrometer and a Waters ACQUITY UHPLC system. Elemental analysis was performed using a FLASH Smart Thermo Elemental analyzer. UV-visible spectra were obtained using a Mortas Scientific UV plus UV-visible spectrophotometer. TGA was performed using a PerkinElmer TGA 4000 instrument. Inductively coupled plasma optical emission spectrophotometry (ICP-OES) analysis was carried out using an AVIO 220 MAX PerkinElmer spectrophotometer. An Elementar Enviro TOC instrument was used to carry out total organic carbon (TOC) analysis. The electron spin resonance (ESR) spectrum was recorded using a Bruker EMX ESP spectrometer. The zeta potentials were recorded using a Nano ZS90 Zeta Sizer by Malvern Panalytical.

2.2. Synthesis of the bis-imine ligand (L₁)

The ONS donor Schiff base ligand (**L₁**) was synthesized following a reported synthetic route.[17]

2.3. Synthesis of the nickel complex [Ni(L₁)(OC₂H₅)]·2H₂O (NiL₁Et)

To a solution of 0.5 mmol **L₁** in ethanol, a 0.5 mmol solution of nickel(II) chloride hexahydrate (NiCl₂·6H₂O) in ethanol was added and stirred. Two drops of triethylamine were added and then allowed to reflux for 8 hours. The **NiL₁Et** complex was obtained as an orange-coloured precipitate. Cooling, followed by filtration, yielded the orange precipitate, which was then rinsed with methanol and then with deionized water. Later, the precipitate was dried in an oven.

Yield: 61.22%. Melting point >300 °C. Observed FT-IR peaks (ν, cm⁻¹): 3398 (O–H stretching vibrations of uncoordinated H_2O), 3048 (sp² C–H stretching vibrations), 2919 (sp³ C–H stretching), 1596 (C=N stretching), 1188 (C–O stretching), 821 (C–S stretching of thiophene ring) (Fig. S1). ^1H NMR (400 MHz, CDCl₃), δ (ppm): 10.27, 8.66, 8.15, 7.92, 7.84, 7.56, 7.10, 6.60, 6.46, 6.12, 4.74, 1.83, 1.24 (Fig. S2). UV-visible (DMSO, λ_{max}, nm): 319, 376, 398, 446, 538 [Fig. S3]. ESI-MS (m/z): calculated for $C_{18}H_{19}BrN_2NiO_4S$ [M]⁺: 495.9602, found: 495.6107 (Fig. S4).

Elemental analysis (%) calculated (found) for $C_{18}H_{19}BrN_2NiO_4S$: C, 43.41 (43.38); H, 3.85 (3.87); N, 5.63 (5.60); S, 6.44 (6.41).

2.4. Theoretical analysis

NiL₁Et was computationally studied employing density functional theory (DFT) using the B3LYP level of theory in the Gaussian 16 program.[18] The optimized geometry of the **NiL₁Et** complex was analyzed using a 6-311++G(d,p) basis set for the ligand and LANL2DZ effective core potential (ECP) for Ni.[19]

2.5. Photocatalytic degradation of dyes

NiL₁Et was screened for its potential photocatalytic activity in the degradation of organic dyes. The widely used cationic dye, Methylene blue (MB), was used to assess the photocatalytic performance of the Ni(II) complex. **NiL₁Et** was added to a 50 mL MB solution. Different volumes of H_2O_2 were then added to this solution. The initial absorbance of the MB dye solution was recorded. Then, the solution was kept away from light for 30 minutes, giving it enough time to reach adsorption–desorption equilibrium. After 30 minutes, the absorbance of the solution was noted again. Then, the MB solution in the presence of **NiL₁Et** was mechanically stirred under direct sunlight. An aliquot of 5 mL was drawn every 10 min, and its absorbance was recorded. The experiments were conducted under direct natural sunlight from 9 am to 12 noon on bright sunny days in the month of September in Silchar, India. The strength of the sunlight was found to vary between 690 W m^{-2} and 770 W m^{-2} when measured using a solar power meter. The catalyst doses varied from 0.2 to 1 g L^{-1}, while the concentration of MB varied over a range of 10 to 30 ppm. The photocatalytic degradation of another cationic dye, Rhodamine B, and an anionic methyl orange dye was performed using a similar procedure.

The degradation efficiency of the dyes was calculated using the following equation:

$$\text{Degradation efficiency (\%)} = \left(\frac{C_0 - C}{C_0}\right) \times 100 \quad (1)$$

where C_0 is the concentration of MB before the beginning of the degradation process, and C is the MB concentration of the aliquots taken at fixed time intervals.

The reaction kinetics of the methylene blue degradation using **NiL₁Et** as the photocatalyst were studied using the following equation:
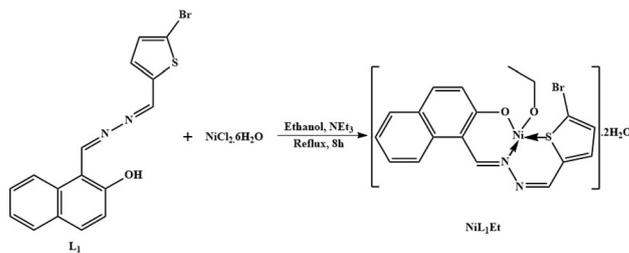
$$\ln \frac{C_0}{C} = kt \quad (2)$$

where C_0 is the initial concentration of MB at time $t = 0$, while C is the concentration of MB at time t, and k is the rate constant.

3 Results and discussion

3.1. Synthesis of NiL1Et

NiL₁Et was obtained from nickel chloride hexahydrate and L_1 in ethanol in the presence of triethylamine (Scheme 1). **NiL₁Et** was found to be soluble in DMSO and DMF.

Scheme 1 Synthesis of $[Ni(L_1)(OC_2H_5)]\cdot 2H_2O$.

3.2. FT-IR spectral study

The formation of **NiL₁Et** was ascertained by comparing the bond vibrations in the FT-IR spectra of **NiL₁Et** and ligand L_1. FT-IR also revealed the binding sites of the metal to the Schiff base. The O–H stretching vibration of L_1, which was visible at 3576 cm^{-1}, was missing in the spectrum of **NiL₁Et**, which indicated the binding of the phenolate to the Ni(II) ion (Fig. S1).[17] A shift in the C–O stretching band to a lower wave number, from 1182 cm^{-1} to 1188 cm^{-1}, was observed when comparing the spectra of the ligand (L_1) and **NiL₁Et**. This further validates the bond formation between the metal and the phenoxide moiety of L_1.[20] Moreover, the presence of uncoordinated water molecules is indicated by the broad band observed at 3398 cm^{-1} in the FT-IR spectrum of **NiL₁Et**.[21,22] The bands at 3048 and 2919 cm^{-1} in the FT-IR spectrum of **NiL₁Et** can be attributed to the aromatic C–H stretching and sp^3 C–H stretching vibrations, respectively.[23] When the spectrum of L_1 was compared to that of **NiL₁Et**, a shift in the C=N stretching vibrations from 1599 cm^{-1} to 1596 cm^{-1} was observed. This reduction in the wave number of C=N stretching vibrations indicates the binding of Ni(II) ions to the imine group of L_1 in the **NiL₁Et** complex.[14] Similarly, a shift in the C–S stretching vibration of the thiophene ring from 829 cm^{-1} in L_1 to 821 cm^{-1} in **NiL₁Et** was observed; this validates the binding between the Ni(II) ion and the S atom of the thiophene ring.[24]

3.3. ¹H nuclear magnetic resonance analysis

Comparing the ¹H-NMR spectrum of L_1 to that of the **NiL₁Et** complex, it was observed that the proton signal for the phenolic OH group was missing in the ¹H-NMR spectrum of **NiL₁Et**. This observation further confirms the binding of Ni(II) to the OH moiety of ligand L_1 (Fig. S2). The proton signal of the imine group that was observed at δ 9.63 for L_1 shifted to δ 10.27 in the ¹H NMR spectrum of **NiL₁Et**, thereby confirming the binding of Ni(II) to the >C=N moiety.[25] Additionally, the ¹H NMR spectrum of **NiL₁Et** exhibits two proton signals at δ 4.74 and δ 1.24 corresponding to the –O–CH₂ and –CH₃ protons, respectively.

3.4. ESI-MS spectral study

The formation of **NiL₁Et** was further confirmed *via* mass spectrometry (Fig. S4). The spectrum exhibits the molecular ion $[M]^+$ peak of $[Ni(L_1)(OC_2H_5)]\cdot 2H_2O$ at an m/z value of 495.6107, which is in close agreement with the calculated value of

495.960. The base peak at an m/z value of 341.1244 corresponds to the $[L_1-OH]^+$ peak of the Schiff base L_1.

3.5. UV-visible spectral study

Upon comparing the UV-visible spectra of L_1 and NiL_1Et using DMSO as the solvent, it was discovered that the ligand (L_1) had $\pi \rightarrow \pi^*$ transitions at λ_{max} 336 and 399 nm,[17] showing hypsochromic shifts to 319 and 376 nm, respectively, after binding to Ni(II) in NiL_1Et (Fig. S3). Another absorption peak at 398 nm was observed, corresponding to the n $\rightarrow \pi^*$ transition of the imine moiety in NiL_1Et.[26] Moreover, two additional absorption bands at 446 and 538 nm corresponding to $^1A_{1g} \rightarrow {}^1B_{1g}$ and $^1A_{1g} \rightarrow {}^1A_{2g}$ (d–d) transitions were observed in the spectrum of NiL_1Et. These bands in the absorption spectrum of NiL_1Et are indicative of a square planar geometry.[14]

3.6. Thermal study

The thermal stability of the NiL_1Et complex was analyzed by thermogravimetric analysis (TGA) in an open atmosphere at a heating rate of 10 °C min^{-1}. A loss of 7.57% from 53 °C to 144.5 °C was noted in the TGA curve (Fig. S5), corresponding to the loss of two uncoordinated H_2O molecules from the complex.[27] A weight loss of 15.87% was recorded within the temperature range of 236 °C to 397 °C for the loss of Br.[28–31] This was followed by the breakdown of the ligand at 447 °C.

3.7. Tauc plot

The UV-DRS analysis of NiL_1Et was performed within the range of 200 to 800 nm (Fig. S6), and the Tauc plot was subsequently obtained (Fig. 1). The Tauc plot was crucial in the determination of the direct band gap of NiL_1Et (E_g), which was 2.19 eV.

3.8. Computational analysis

The most probable geometry of NiL_1Et was optimized using DFT, and the electronic properties, stability, and reactivity of the complex were studied theoretically. The optimization yielded a square planar geometry for the NiL_1Et complex, where the O17, N19, and S29 of the ligand (L_1) were bonded to the Ni(II) center (Fig. 2). The O31 of $-OC_2H_5$ completed the fourth coordination site of the square planar geometry. The O17–Ni–N19, N19–Ni–S29, S29–Ni–O31, and O31–Ni–O17 bond angles were found to be 95.50°, 92.41°, 83.40°, and 97.93°, respectively. The bond lengths of O17–Ni, N19–Ni, S29–Ni, and O31–Ni were found to be 1.858 Å, 1.999 Å, 2.326 Å, and 1.793 Å, respectively. The computational determination of the HOMO and LUMO energies revealed that NiL_1Et has a HOMO–LUMO energy gap of 2.4325 eV, which is in close agreement with the value of the direct band gap obtained using the Tauc plot (Fig. 3). The HUMO and LUMO energies of NiL_1Et were −5.1780 eV and −2.7455 eV, respectively. The HOMO and LUMO energies of the complex were crucial in determining the electronegativity (χ), ionization potential (IP), chemical potential (μ), electron affinity (EA), global hardness (η), global electrophilicity (ω), and global softness (σ) (Table 1). NBO analysis revealed that the formal charge on Ni(II) decreased to +0.889 after complexation, which indicated the bonding of Ni(II) to the ligand, resulting in the transfer of electrons from the ligand to the Ni(II) center in NiL_1Et.

3.9. Photoluminescence analysis to determine the electron–hole recombination rate

The change in the intensities of the emissions observed in the photoluminescence (PL) spectrum is crucial in estimating the recombination rate of charge carriers (e^-–h^+ pair).[32–34] Higher emission intensities indicate a higher recombination rate of the electron–hole pairs, while lower emission intensities indicate a slower recombination of the electron–hole pairs. A lower electron–hole recombination rate suggests better photocatalytic efficiency.[33,35] The PL spectra of L_1 and NiL_1Et reveal a comparatively higher emission intensity for the ligand (L_1), while the photoluminescence intensity of NiL_1Et was much lower (Fig. 4).
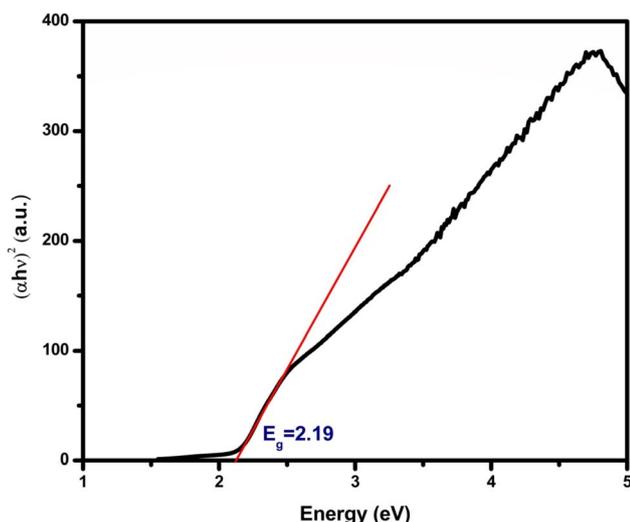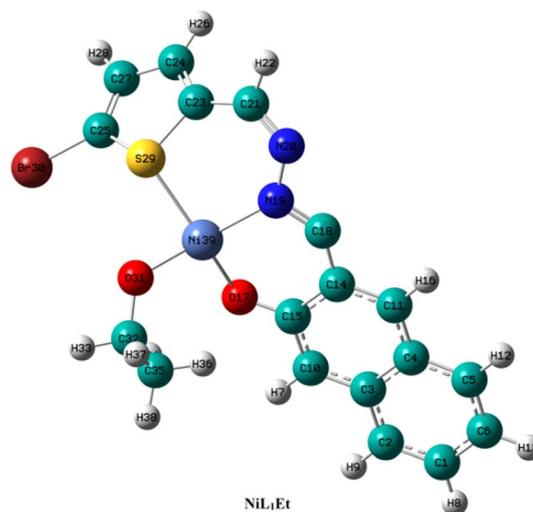

Fig. 1 Tauc plot of the NiL_1Et complex.

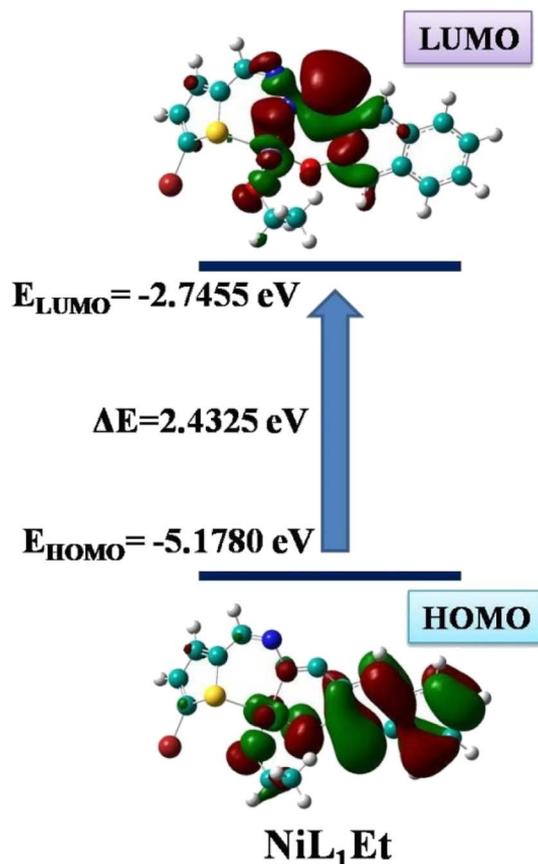Fig. 2 Optimised structure of the NiL_1Et complex.

© 2026 The Author(s). Published by the Royal Society of Chemistry

Paper

Fig. 3 HOMO and LUMO energies of the NiL$_1$Et complex.

Table 1 Global reactivity descriptors of the NiL$_1$Et complex

Parameters	NiL$_1$Et
E_{HOMO} (eV)	−5.1780
E_{LUMO} (eV)	−2.7455
ΔE (eV)	2.4325
IP (eV)	5.1780
EA (eV)	2.7455
χ (eV)	3.96175
μ (eV)	−3.96175
η (eV)	1.21625
σ (eV^{-1})	0.41109
ω (eV)	6.4524

Thus, **NiL$_1$Et** can be expected to have much slower charge carrier recombination; therefore, **NiL$_1$Et** is expected to exhibit desirable photocatalytic activity.

3.10. Photocatalytic Methylene blue (MB) degradation

3.10.1. Effect of catalyst dosage. The extent of degradation of methylene blue was analyzed with varying photocatalyst amounts ranging from 0.2 to 1 g L^{-1}. In this experiment, a 20 ppm solution of MB in 50 mL of deionized water in the presence of 20 μL of H$_2$O$_2$ was placed under direct sunlight while maintaining the pH at 7. The maximum
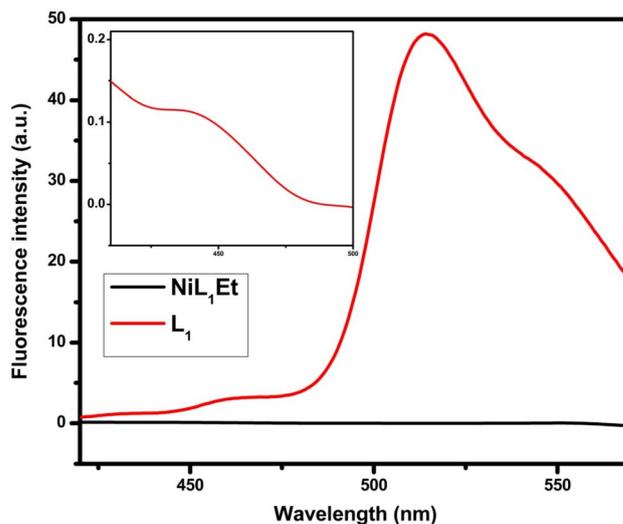
Fig. 4 Photoluminescence spectra of L$_1$ and the NiL$_1$Et complex. Inset: zoomed photoluminescence spectrum of L$_1$.

photodegradation efficiency obtained using **NiL$_1$Et** was found to be 76.39% at a catalyst dose of 0.8 g L^{-1} (Fig. 5(a)). The kinetics of the reaction using varying catalyst dosages were determined (Fig. 5(b)). The photocatalytic MB degradation was found to follow pseudo-first-order kinetics, as $R^2 > 0.95$. The rate constant had a maximum value of 0.0233 min^{-1} for 0.8 g per L **NiL$_1$Et**.

3.10.2. Effect of methylene blue concentration. The concentrations of MB taken initially for the degradation experiments were optimized with different concentrations of MB, starting from 10 to 40 ppm. The dose of **NiL$_1$Et** was fixed at 0.8 g L^{-1}. The MB solution was added to 20 μL of H$_2$O$_2$ while maintaining the pH at 7. The maximum degradation was achieved with an MB concentration of 20 ppm (Fig. 6(a)). The photodegradation efficiency decreased when the initial concentration of MB exceeded 20 ppm, which can again be attributed to reduced light penetration, decreasing the path length of photons entering the MB solution at higher initial concentrations. Moreover, the percentage of degradation of MB falls with a rise in the MB concentration exceeding 20 ppm, as the degradation of a higher initial concentration of MB requires a higher catalyst surface, but in this study, the catalyst dose of **NiL$_1$Et** was fixed.[36] The kinetics study revealed that (Fig. 6(b)) the rate constant was maximum (0.0229 min^{-1}) at an initial MB concentration of 20 ppm for **NiL$_1$Et**.

3.10.3. Effect of H$_2$O$_2$ dosage. Volumes of H$_2$O$_2$ ranging from 0 to 80 μL were added to evaluate its effect on the degradation efficiency. A 50 mL solution of 20 ppm MB in deionized water was irradiated with sunlight in the presence of 0.8 g L^{-1} **NiL$_1$Et**. The pH of 7 was maintained throughout the experiment (Fig. 7(a) and (b)). The degradation efficiency was enhanced with increasing H$_2$O$_2$ volumes; however, a gradual fall in the efficiency was observed when H$_2$O$_2$ volumes higher than 40 μL were added. The rise in the degradation efficiency in the presence of H$_2$O$_2$ is mainly due to the self-decomposition of H$_2$O$_2$ to
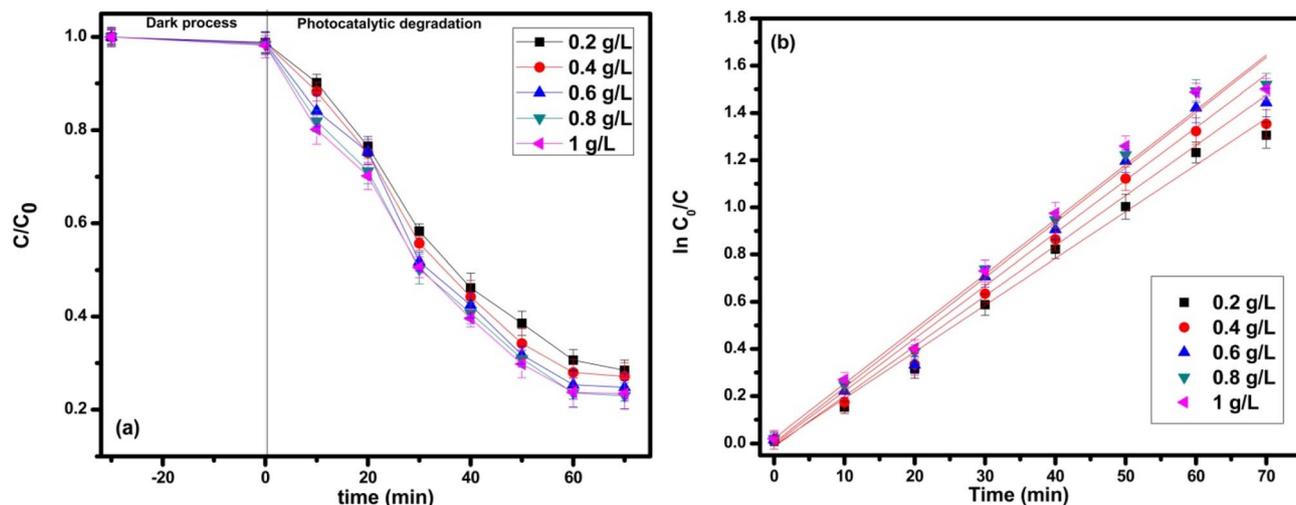
Fig. 5 (a) Plot of C/C_0 vs. time. (b) Reaction kinetics of the photodegradation of MB using varying doses of the NiL_1Et complex.

produce hydroxy radicals ($\cdot OH$) when irradiated with sunlight. Moreover, the fall in efficiency when the added volume of H_2O_2 exceeded 40 μL was due to the scavenging of the reactive hydroxy radicals ($\cdot OH$) by excess H_2O_2 molecules to produce $\cdot O_2H$ radicals, which are less active than $\cdot OH$ radicals.[37]

3.10.4. Effect of change in pH. The effects of pH on the photodegradation of MB were evaluated by varying the pH from 5 to 11. A 20 ppm solution of MB was taken, and the catalyst dose of 0.8 g per L NiL_1Et was added, followed by the addition of 40 μL of H_2O_2. The degradation efficiency increased with an increase in pH from 5 to 11 (Fig. 8(a)). At a pH greater than 7, the surface of the photocatalyst is negatively charged, and as MB is a cationic dye, the electrostatic interaction between the cationic MB dye and the negatively charged catalyst surface is enhanced. This is what causes the increase in the photodegradation efficiency at a higher pH.[38] Moreover, at a pH greater than 7, an enhanced adsorption of the cationic MB dye on the catalyst

surface is expected.[39] The increased adsorption of MB on the catalyst surface further enhances the photodegradation of MB at a higher pH.[40] The kinetics of the degradation were studied (Fig. 8(b)). The rate of degradation at a pH of 11 was found to be 0.02569 min^{-1} using NiL_1Et. This shows that a higher pH is desirable for better degradation of the MB dye. However, the study also indicates that NiL_1Et can degrade the MB dye even under neutral conditions, although the efficiency is lower than that obtained at a pH of 11.

The zeta potential analysis of the catalyst was performed to examine its surface charge at different pH levels. The pH of the point zero charge (pH_{ZPC}) of NiL_1Et was found to be 6.46. The zeta potentials at $pH < pH_{ZPC}$ were found to be positive, indicating that the catalyst surface is positively charged at $pH < pH_{ZPC}$, thereby attracting negatively charged molecules. The zeta potentials at $pH > pH_{ZPC}$ were found to be negative; this
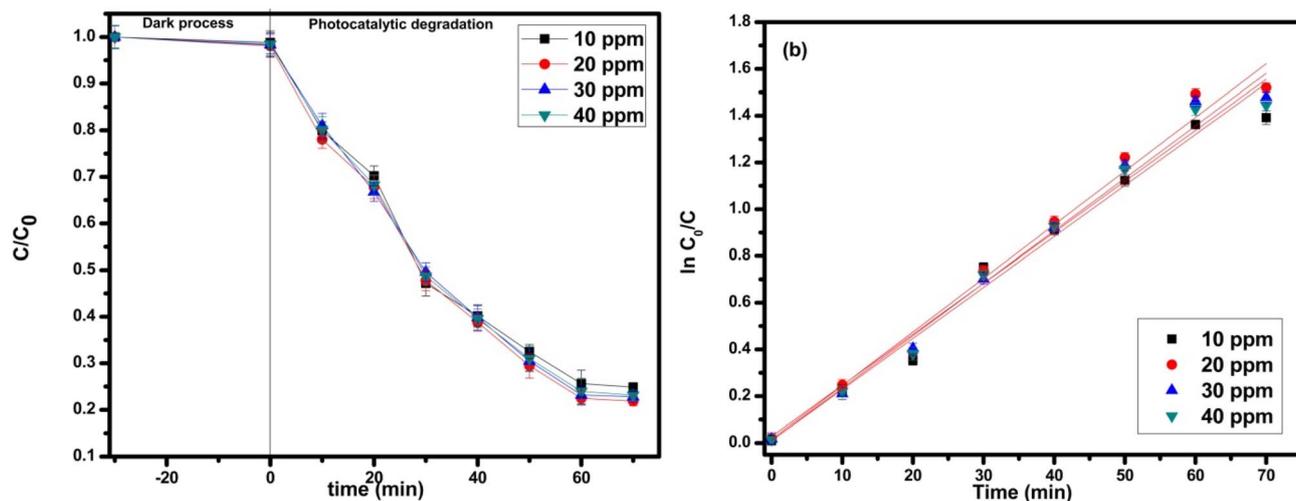

Fig. 6 (a) Plot of C/C_0 vs. time. (b) Reaction kinetics of the photodegradation with varying initial concentrations of MB in the presence of the NiL_1Et complex.
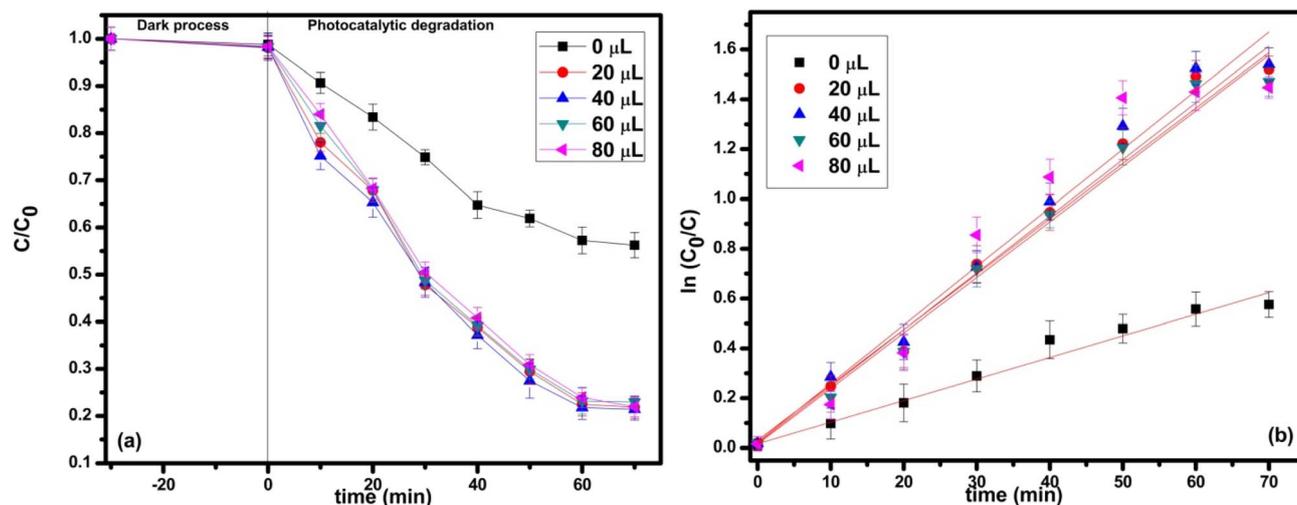
Fig. 7 (a) Plot of C/C_0 vs. time. (b) Reaction kinetics of the photodegradation of MB at different H_2O_2 dosages in the presence of the NiL_1Et complex.

indicates that the catalyst surface is negatively charged at pH > pH_{ZPC}, which will attract cationic molecules (Fig. S7).[35,41]

3.10.5.   Effect of reaction time. The time required to achieve the maximum possible MB degradation efficiency was evaluated. The optimum catalyst dose was 0.8 g per L NiL_1Et. A 20 ppm solution of MB in 50 mL of deionized water, maintained at a pH of 11, was irradiated with sunlight in the presence of 40 μL of H_2O_2. After 60 minutes, a degradation efficiency of 80.15% was achieved using NiL_1Et as the catalyst. No notable enhancement in degradation efficiency was observed beyond 60 min (Fig. 8(a)). Fig. S8 presents the absorption spectra of the photocatalytic degradation of MB under optimized conditions in the presence of NiL_1Et as the photocatalyst. The effectiveness of this degradation procedure using NiL_1Et as the photocatalyst under sunlight was further analysed by performing the dye degradation experiment under specific controlled conditions, such as degradation in the presence of only H_2O_2 in the dark,

NiL_1Et and H_2O_2 in the dark, only H_2O_2 under sunlight, and only NiL_1Et without H_2O_2 under sunlight (Fig. S9). Upon comparing the degradation efficiencies achieved under the different conditions, it was discovered that NiL_1Et in the presence of H_2O_2 under sunlight is the required condition to obtain the maximum possible degradation efficiency.

A comparison of the photocatalytic efficiencies of NiL_1Et in the degradation of MB and those of some reported Ni(II) Schiff complexes is presented in Table 2. It was observed that a fairly high degradation efficiency was achieved using NiL_1Et under direct sunlight when compared to other Ni(II) Schiff base complexes. The degradation of MB using NiL_1Et was also compared with some of the reported nanomaterials used to obtain high degradation efficiency. It was observed that the degradation efficiency achieved by NiL_1Et in a relatively shorter period is also in a comparable range to those of some Ni(II) Schiff base complexes, which achieved higher degradation
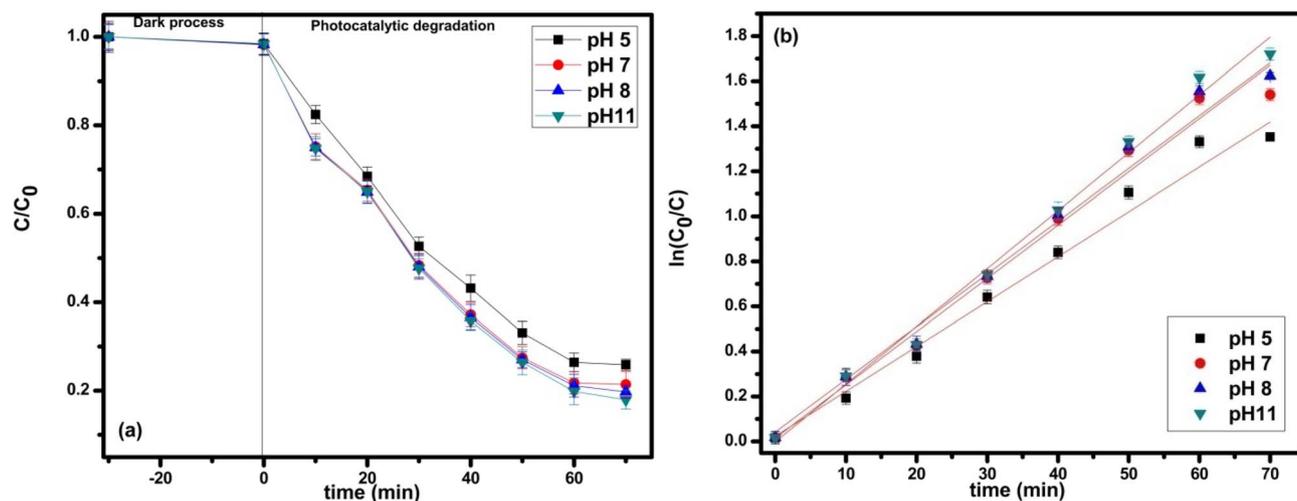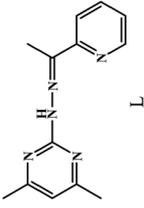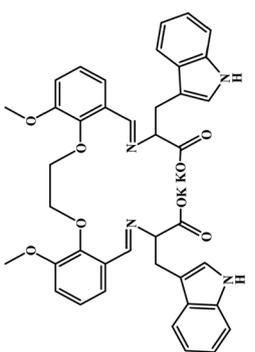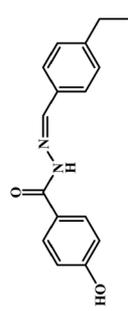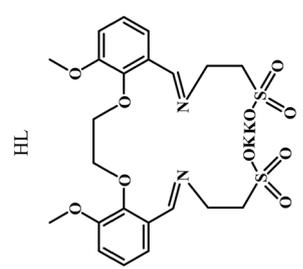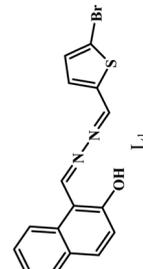

Fig. 8 (a) Plot of C/C_0 vs. time. (b) Reaction kinetics of the photodegradation of MB at different pH levels using the NiL_1Et complex.

Table 2 Comparison of the degradation efficiencies of the NiL₁Et complex and some reported Ni(ɪɪ) Schiff base complexes

Complex/catalyst	Ligand	Degradation efficiency	Irradiation time	References
[Ni(HL)L]Cl·2CH₃OH·4H₂O [Ni(HL)L]NO₃·3H₂O [Ni(HL)L]Br·4H₂O	quinoline-2-carbaldehyde-N(4)-cyclohexylthiosemicarbazone	47% 58% 55%	60 min under visible light 60 min under visible light 60 min under visible light	12
Ni-ABzC	ABzC	62.50%	40 min under sunlight	14
[Ni(PL)₂]	PL	72.35%	12 hours	43
Ni(ɪɪ)-Schiff base complex	(1E,1′E)-N¹,N′′-((3E,3′E)-(1,4-phenylenebis(azanylylidene))bis(1,5-dimethyl-2-phenyl-2,3-dihydro-1H-pyrazole-4-yl-3-ylidene))diacetimidamide	74.60%	Under UV lamp	44
SBLNi	SBL	76.80%	200 min under UV lamp	45

Table 2 (*Contd.*)

Complex/catalyst	Ligand	Degradation efficiency	Irradiation time	References
$[Ni^{II}(L)_2][ClO_4)_2] \cdot 2H_2O$	L	84.50%	120 min under UV light	46
$Ni(C_{40}H_{36}N_4O_8) \cdot 3CH_3OH$		85%	100 min under Hg lamp	47
$[Ni(HL)_2]$	HL	91% at pH = 12	60 min under UV light	15
$[Ni(C_{22}H_{26}N_2O_{10}S_2)] \cdot 2CH_3OH$		95.49%	140 min under Hg lamp	16
NiL_1Et	L_1	80.15%	60 min under sunlight	This work
Green-synthesized $CoFe_2O_4/TiO_2$ nanocomposites	—	98.70%	20 min under UV irradiation	48
TiO_2 nanotubes	—	87%	300 min under UV irradiation	49
ZnO/Fe_2O_4 heteronanostructures	—	99.70%	150 min under UV and visible light	50
$BiFeO_3$ nanoparticles	—	99%	15 min under 450 W mercury vapour lamps	51

efficiencies. Although using the nanomaterials as photocatalysts yielded higher degradation efficiencies, **NiL₁Et** was capable of degrading MB comparatively within a shorter period in most cases. Furthermore, the degradation of MB using **NiL₁Et** was carried out following a more sustainable approach, using direct natural sunlight. This approach is cost-efficient and user-friendly, as no additional instrumentation or artificial power source is required. In contrast to this, the degradation of MB using some of the reported Ni(II) Schiff base complexes and the majority of the nanomaterials compared in Table 2 was performed under irradiation from artificial light sources like a UV or Hg lamp, which will require additional electricity. This can, in turn, be challenging for the application of such catalytic species in large-scale studies or in real, practical applications.

However, while determining the degradation efficiency of a photocatalyst, estimating only the discoloration of the organic dye is not enough; for a degradation process to be effective, it is essential that it causes the mineralization of the dye too. The mineralization of methylene blue (MB) was assessed through TOC analysis. Methylene blue (MB), having the molecular formula $C_{16}H_{18}N_3SCl$, has a carbon fraction of 0.6007.[42] Thus, the initial 20 ppm MB solution has a TOC value of 12.014 mg L^{-1}. The degraded MB solution using **NiL₁Et** after 60 min of irradiation under sunlight has a final TOC value of 4.19 mg L^{-1}. This indicated that **NiL₁Et** in the presence of H_2O_2 under sunlight could not only cause the discoloration of the MB solution, but it could also mineralize the MB dye with a 65.12% TOC removal.[43–51]

3.11. Photocatalytic degradation of Rhodamine B (Rh B) and methyl orange (MO) dyes

To fully understand the broader potential of the Ni(II) complex, **NiL₁Et**, as a photocatalyst for the degradation of organic dyes in an aqueous environment, the photocatalytic degradation of
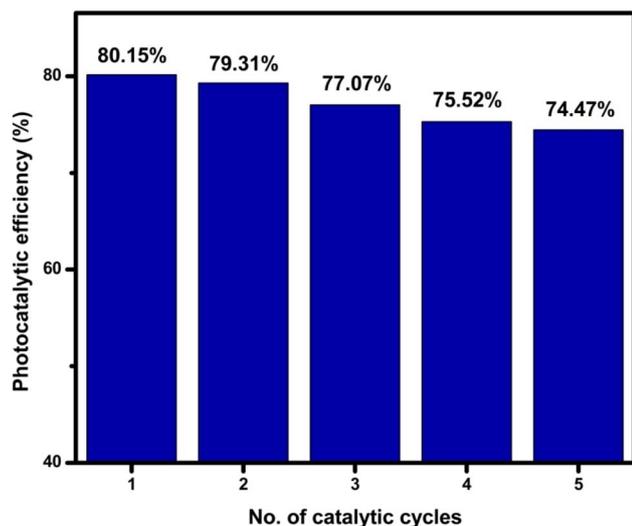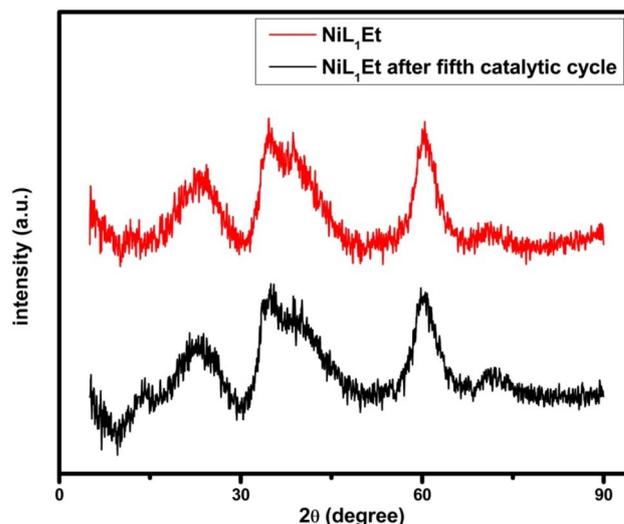

Fig. 10 XRD patterns of the freshly prepared **NiL₁Et** complex and after the fifth catalytic cycle in the photodegradation of MB, collected at a scan rate of 0.071112° per second.

other cationic and anionic dyes was also investigated. Rhodamine B (Rh B) was used as the other cationic dye, and methyl orange was used as an anionic dye.[52,53] 20 ppm solutions of both dyes were treated with 0.8 g L^{-1} **NiL₁Et** in the presence of 40 μL of H_2O_2 under sunlight under neutral conditions. Moreover, degradation experiments were carried out separately in the presence of only H_2O_2 in the dark, in the presence of both **NiL₁Et** and H_2O_2 in the dark, in the presence of only H_2O_2 under sunlight, and in the presence of only **NiL₁Et** under sunlight (Fig. S10(a) and S11(a)). Degradation efficiencies of 77.33% after 80 min of irradiation and 54.85% after 120 min of irradiation were achieved while degrading the RhB and MO dyes, respectively (Fig. S10(b) and S11(b)). Thus, it was observed that **NiL₁Et** as a photocatalyst under sunlight is capable of achieving higher efficiency against cationic dyes as compared to anionic dyes. This observation is in agreement with the results of the zeta potential experiment. As **NiL₁Et** has a negatively charged surface at a neutral pH, cationic dyes will be more attracted to the catalyst surface compared to anionic dyes, resulting in better degradation efficiency in the case of cationic dyes.[35]

3.12. Recyclability, stability, and leaching studies of the catalyst

The ability to reuse and recycle the catalyst in consecutive catalytic cycles is essential for cost-effective and feasible practical applications. This is also indicative of the structural stability of the catalyst species under reaction conditions. The used catalyst was recovered by centrifugation, followed by thorough rinsing with deionised water. The recovered catalyst was then dried in a hot air oven before reuse in the next catalytic cycle. **NiL₁Et** was used consecutively for five catalytic cycles (Fig. 9). Even after the fifth catalytic cycle, only a minute fall in the degradation efficiency of MB was noted. This fall in the efficiency of the photocatalytic degradation of MB after five

Fig. 9 Recyclability of the **NiL₁Et** complex as a catalyst in the photodegradation of MB.

consecutive cycles using the recovered **NiL$_1$Et** catalyst can be attributed to the blocking of some of the active sites on the **NiL$_1$Et** surface by the produced degradation intermediates.[35]

The stability of **NiL$_1$Et** in the reaction medium was further analyzed by comparing the FT-IR spectrum and XRD pattern of **NiL$_1$Et** before using it in the catalytic process and after the fifth consecutive catalytic cycle. All the peaks of the FT-IR spectrum of **NiL$_1$Et** recorded after the fifth catalytic cycle (Fig. S12) matched the FT-IR spectrum of the freshly prepared **NiL$_1$Et**. This indicated the high structural stability of **NiL$_1$Et** as the photocatalyst during the MB degradation process. A similar conclusion can be drawn when the diffraction pattern of the freshly prepared **NiL$_1$Et** was compared to that of the recovered **NiL$_1$Et** after the fifth consecutive catalytic cycle (Fig. 10). Both the diffraction patterns were identical. This further established the fact that **NiL$_1$Et** is a stable photocatalytic species where the reaction conditions had no significant effect on its structural integrity.

Furthermore, a leaching study was conducted using ICP-OES on the sample collected after the catalytic cycle. The mass of Ni leached after the catalytic cycle was 25.09 µg L^{-1} (25.09 × 10^{-6} g L^{-1}). Thus, the percentage leaching of Ni was 0.02%, which was negligible. Moreover, the obtained value of leaching Ni mass was well below the WHO-recommended limit of 70 µg L^{-1} in drinking water.[54]

3.13. Photocatalytic mechanism

To determine the photocatalytic mechanism, it is crucial to identify the active species responsible for dye degradation. Thus, to identify the reactive oxygen species generated during the photocatalytic degradation of MB, a radical-scavenging experiment was performed. During this experiment, the degradation of MB in the presence of various radical scavengers was studied. Here, potassium persulphate (K$_2$S$_2$O$_8$), disodium EDTA (Na$_2$EDTA), benzoic acid, and ascorbic acid were employed as scavengers for e$^-$, h$^+$, ·OH, and ·O$_2^-$, respectively.[35,55] It was observed that in the photocatalytic degradation of MB using **NiL$_1$Et** as the catalyst, in the presence of potassium persulphate (K$_2$S$_2$O$_8$), disodium EDTA (Na$_2$EDTA), benzoic acid, and ascorbic acid, the degradation efficiency falls to 65.05%, 60.09%, 22.11%, and 53.61%, respectively (Fig. S13). These observations suggested that hydroxyl radicals (·OH) were the dominant active species in the degradation of MB.
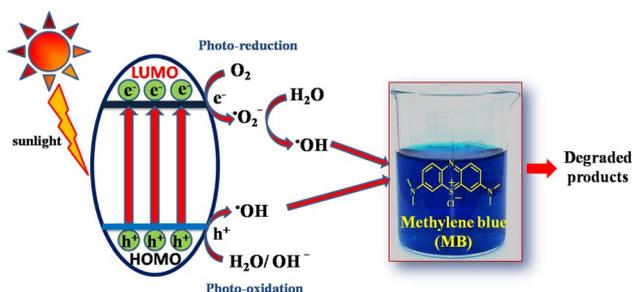

Fig. 11 Schematic of the mechanism of the photocatalytic degradation of MB using **NiL$_1$Et** as the catalyst.

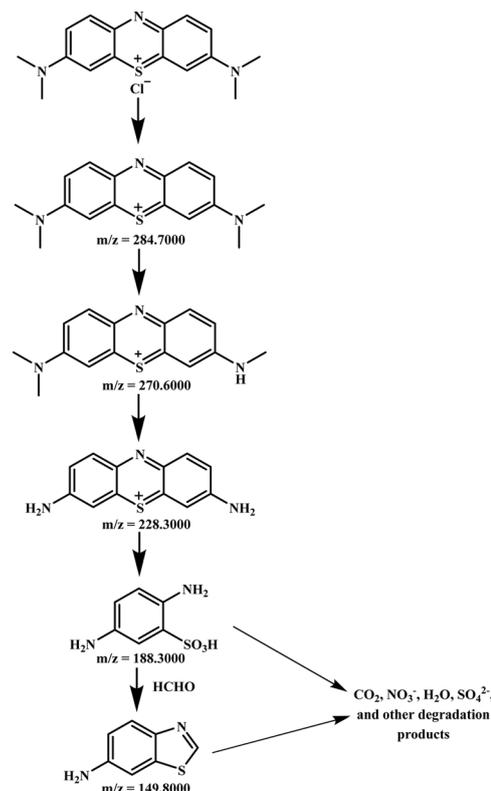**Fig. 12** Probable degradation pathway of MB.

Furthermore, the generation of hydroxy radicals (·OH) was confirmed via an ESR spin trapping experiment. α-Phenyl-*N*-*tert*-butylnitrone (PBN) was used as the spin trapping agent. The obtained ESR spectrum matched the characteristic spectrum of the reported PBN–·OH adduct (Fig. S14). The obtained hyperfine splitting constants (HFSCs) a_N = 15.39 G and a_H = 2.86 G are in agreement with the reported HFSCs for PBN–·OH adducts.[56,57] This confirms the generation of hydroxy radicals (·OH) as the reactive oxygen species during the degradation of the dyes using **NiL$_1$Et** as the photocatalyst.

Thus, correlating the experimental findings with the available literature on the advanced oxidation process, the mechanism of the photocatalytic degradation of MB using **NiL$_1$Et** is expected to involve the transfer of electrons from the HOMO to the LUMO of the catalyst under direct sunlight, as **NiL$_1$Et** has a semiconductor-like low HOMO–LUMO energy gap of 2.19 eV.[58] This excitation of electrons to the LUMO also generates an equal number of holes (h$^+$) in the HOMO of **NiL$_1$Et**. The lower electron–hole recombination rate of **NiL$_1$Et**, as indicated by the low emission intensity in the photoluminescence spectrum, further facilitates this charge separation. Thus, the holes (h$^+$) produced in the HOMO can interact with hydroxyl ions (OH$^-$) or water molecules and oxidize them to produce hydroxy radicals (·OH). The electrons in the LUMO of the catalysts react with the O$_2$ molecules present in the solution and reduce them to ·O$_2^-$ radicals. The ·O$_2^-$ radicals can, in turn, react with the available water molecules to produce hydroxy radicals (·OH).[10,58,59] The produced hydroxy radicals (·OH) can then react with MB

molecules and degrade them to afford degraded products along with H_2O.[59,60] An illustration of the photocatalytic degradation mechanism using **NiL₁Et** as a catalyst is provided in Fig. 11.

Furthermore, the H_2O_2 molecules present in the reaction medium can further dissociate to produce ·OH radicals, leading to an increase in the concentration of ·OH radicals in the reaction medium.[37]

3.14. Photocatalytic degradation pathway of methylene blue

The degradation path of methylene blue (MB) can be traced by identifying the degradation intermediates. A sample was collected during the photocatalytic degradation of MB using **NiL₁Et**, and its LC-MS analysis was conducted to identify the intermediates during the course of the degradation. The corresponding chromatogram and mass spectra are provided in Fig. S15 and S16, respectively. It was observed that the photocatalytic degradation of MB initially involved the demethylation of MB molecules. The demethylated MB molecules then undergo degradation, yielding 2,5-diaminobenzenesulfonic acid as an intermediate. A benzothiazole derivative is also among the degradation intermediates identified in the LC-MS study. A plausible degradation pathway of MB was thus drafted based on the chromatograms and mass spectra of the degradation intermediates of MB degradation, as shown in Fig. 12. The proposed mechanism is in agreement with reported works.[61–63]

4 Conclusion

A new Ni(II) complex, **NiL₁Et,** of an ONS donor ligand (**L₁**) was synthesized. The formation of the complex was confirmed using spectroscopic techniques and elemental analysis. The thermal and optical study of the complex was conducted by TGA and UV-DRS. The energy-optimised geometry of **NiL₁Et** was obtained using DFT calculations. **NiL₁Et** was found to have a distorted square planar geometry. The experimentally determined band gap of 2.19 eV for **NiL₁Et**, computed using Tauc plots, was in close agreement with the theoretically obtained value. The **NiL₁Et** complex was found to have a low electron–hole recombination rate, which can be predicted from its very low emission intensity. The photocatalytic activity of **NiL₁Et** was investigated. The H_2O_2-assisted photocatalytic degradation of methylene blue (MB) occurred at a pH of 11. The degradation efficiency of MB reached the maximum of 80.15% using **NiL₁Et** when 50 mL of a 20 ppm MB solution was irradiated under sunlight. It was also observed that upon irradiation with sunlight and in the presence of the photocatalysts, MB degradation was enhanced with an increase in the pH. The zeta potential analysis was carried out to study the surface potential of the catalyst at different pH levels. The catalyst was found to have a negative surface potential at all pH levels above 6.46. Upon studying the mechanism of the photocatalytic degradation of MB using **NiL₁Et** as the photocatalyst, it was discovered that the hydroxy radicals (·OH) generated during the degradation process were crucial in causing the photocatalytic degradation. Moreover, the mineralization of the MB dye was assessed through TOC

analysis. The efficacy of **NiL₁Et** in the degradation of other cationic dyes, like Rhodamine B, and anionic dyes, like methyl orange, was evaluated. The recyclability and stability of the complex as a photocatalyst were evaluated until the fifth consecutive catalytic cycle. The possible leaching of Ni was screened *via* ICP-OES, and the amount of Ni leached was found to be 25.09 μg L^{-1}, which was well below the WHO-recommended limit for Ni in water. The degradation pathway of MB was traced through the identification of the degradation intermediates using LC-MS.

Author contributions

Nilotpal Goswami: conceptualization, data curation, formal analysis, investigation, methodology, writing – original draft, and visualization. Nabajit Barman: investigation. Pranjit Barman: validation, supervision, and writing – review and editing.

Conflicts of interest

The authors declare no conflict of interest.

Data availability

The data supporting this article have been included as part of the supplementary information (SI). Supplementary information is available. See DOI: https://doi.org/10.1039/d5su00958h.

Acknowledgements

References

1 M. Kumar, S. Ambika, A. Hassani and P. V. Nidheesh, Waste to catalyst: Role of agricultural waste in water and wastewater treatment, *Sci. Total Environ.*, 2023, **858**, 159762, DOI: 10.1016/j.scitotenv.2022.159762.

2 A. Islam, S. H. Teo, Y. H. Taufiq-Yap, C. H. Ng, D. N. Vo, M. L. Ibrahim, M. M. Hasan, M. A. R. Khan, A. S. M. Nur and M. R. Awual, Step towards the sustainable toxic dyes removal and recycling from aqueous solution- A comprehensive review, *Resour., Conserv. Recycl.*, 2021, **175**, 105849, DOI: 10.1016/j.resconrec.2021.105849.

3 L. Liu, L. Cao, H. Niu and J. Wang, Zinc Metal–Organic Framework Growing on the Surface of Fruit Peels and Its Photocatalytic Activity, *ACS Omega*, 2021, **6**, 10187–10195, DOI: 10.1021/acsomega.1c00466.

4 L. H. Abdel-Rahman, K. M. H. Mohammed, M. R. Shehata, E. A. H. Ahmed and A. Nafady, Synthesis and Characterization of New Heterogeneous Catalysts Via Pre-templating of Schiff base Cu (II) Complexes for Efficient

Photo Degradation of Methylene Blue, *Int. J. Nano. Chem.*, 2022, **8**, 1–9.

5 L. Li, J. Wang, Y. Guo, Q. Li, Y. Wang, Y. Bai and D. Dang, Structural diversity in four coordination polymers based on polypyridyl ligand regulated by metal centers for photodegradation of methylene blue and methyl orange, *J. Solid State Chem.*, 2022, **305**, 122664, DOI: 10.1016/j.jssc.2021.122664.

6 J. Kong, A. Li, X. Li, H.-F. Zhai, W. Zhang, Y. Gong, H. Li and D. Wu, Photodegradation of methylene blue using Ta-doped ZnO nanoparticle, *J. Solid State Chem.*, 2010, **183**, 1359–1364, DOI: 10.1016/j.jssc.2010.04.005.

7 G. Jiang, X. Zheng, Y. Wang, T. Li and X. Sun, Photodegradation of methylene blue by multi-walled carbon nanotubes/TiO2 composites, *Powder Technol.*, 2011, **207**, 465–469, DOI: 10.1016/j.powtec.2010.11.029.

8 M. J. Height, S. E. Pratsinis, O. Mekasuwandumrong and P. Praserthdam, Ag-ZnO catalysts for UV-photodegradation of methylene blue, *Appl. Catal., B*, 2006, **63**, 305–312, DOI: 10.1016/j.apcatb.2005.10.018.

9 N. Asghar, A. Hussain, D. A. Nguyen, S. Ali, I. Hussain, A. Junejo and A. Ali, Advancement in nanomaterials for environmental pollutants remediation: a systematic review on bibliometrics analysis, material types, synthesis pathways, and related mechanisms, *J. Nanobiotechnol.*, 2024, 26, DOI: 10.1186/s12951-023-02151-3.

10 N. Goswami and P. Barman, Schiff base metal complexes as alternative heterocatalysts in water remediation: Photocatalytic degradation of toxic organic pollutants, *J. Mol. Struct.*, 2026, **1349**, 143925, DOI: 10.1016/j.molstruc.2025.143925.

11 P. H. F. Fasna, S. Sasi, T. K. B. Sharmila, C. S. J. Chandra, J. V. Antony and V. Raman, Photocatalytic remediation of methylene blue and antibacterial activity study using Schiff base-Cu complexes, *Environ. Sci. Pollut. Res.*, 2022, **29**, 54318–54329.

12 A. Mohan, L. V. Menon, K. K. M. Hashim and E. Manoj, Synthesis, characterization, and theoretical studies of three similar nickel(II) complexes: Biological and photocatalytic applications, *Polyhedron*, 2025, **274**, 117499, DOI: 10.1016/j.poly.2025.117499.

13 H. R. Mardani, A. Esmaeili and A. Malekzadeh, Comparative study of bis-chelate M(II) complexes (M=Ni, Cu, Zn) as new heterogeneous photocatalysts for degradation of methylene blue under visible light, *Res. Chem. Intermed.*, 2018, **44**, 6183–6195, DOI: 10.1007/s11164-018-3484-z.

14 H. P. Gogoi, N. Goswami, A. Singh and P. Barman, Microwave-assisted synthesis of Schiff base metal complexes: Biological, photocatalytic activity and fabrication of their metal oxide nanoparticles, *J. Mol. Struct.*, 2024, **1303**, 137583, DOI: 10.1016/j.molstruc.2024.137583.

15 N. B. G. Reddy, P. M. Krishna and N. Kottam, Novel metal-organic photocatalysts: Synthesis, characterization and decomposition of organic dyes, *Spectrochim. Acta, Part A*, 2015, **137**, 371–377, DOI: 10.1016/j.saa.2014.08.045.

16 H. Wang, X. Meng, C. Fan, Y. Fan and C. Bi, Synthesis, crystal structure, DFT study, and photocatalytic property of a new Ni(II) complex of a symmetric N2O4-donor bis-Schiff base ligand, *J. Mol. Struct.*, 2016, **1107**, 25–30, DOI: 10.1016/j.molstruc.2015.11.035.

17 N. Goswami, H. P. Gogoi and P. Barman, A hydrazine-based unsymmetrical bis-imine-Schiff base as a chemosensor for turn-off fluorescence and naked-eye detection of Cu2+ ion: Application in aqueous media using test strips, *J. Photochem. Photobiol., A*, 2024, **446**, 115106, DOI: 10.1016/j.jphotochem.2023.115106.

18 M. J. Frisch, G. W. Trucks, H. B. Schlegel, G. E. Scuseria, M. A. Robb, J. R. Cheeseman, G. Scalmani, V. Barone, G. A. Petersson, H. Nakatsuji, X. Li, M. Caricato, A. V. Marenich, J. Bloino, B. G. Janesko, R. Gomperts, B. Mennucci, H. P. Hratchian, J. V. Ortiz, A. F. Izmaylov, J. L. Sonnenberg, D. Williams-Young, F. Ding, F. Lipparini, F. Egidi, J. Goings, B. Peng, A. Petrone, T. Henderson, D. Ranasinghe, V. G. Zakrzewski, J. Gao, N. Rega, G. Zheng, W. Liang, M. Hada, M. Ehara, K. Toyota, R. Fukuda, J. Hasegawa, M. Ishida, T. Nakajima, Y. Honda, O. Kitao, H. Nakai, T. Vreven, K. Throssell, J. A. Montgomery Jr, J. E. Peralta, F. Ogliaro, M. J. Bearpark, J. J. Heyd, E. N. Brothers, K. N. Kudin, V. N. Staroverov, T. A. Keith, R. Kobayashi, J. Normand, K. Raghavachari, A. P. Rendell, J. C. Burant, S. S. Iyengar, J. Tomasi, M. Cossi, J. M. Millam, M. Klene, C. Adamo, R. Cammi, J. W. Ochterski, R. L. Martin, K. Morokuma, O. Farkas, J. B. Foresman, and D. J. Fox, *Gaussian 16 Rev. C.01*, Wallingford, CT, 2016.

19 H. Kargar, M. Ashfaq, M. Fallah-Mehrjardi, R. Behjatmanesh-Ardakani, K. S. Munawar and M. N. Tahir, Synthesis, characterization, SC-XRD, HSA and DFT study of a novel copper(I) iodide complex with 2-(thiophen-2-yl)-4,5-dihydro-1H-imidazole ligand: An experimental and theoretical approach, *J. Mol. Struct.*, 2022, **1253**, 132264, DOI: 10.1016/j.molstruc.2021.132264.

20 C. E. Satheesh, P. Raghavendra Kumar, P. A. Suchetan, H. Rajanaika and S. Foro, New (N, O) Schiff bases of 2-hydroxynaphthaldehyde and their homoleptic Zn(II) and Cu(II) complexes – Synthesis, structural characterization, Hirshfeld surface analysis and antimicrobial activity studies, *Inorg. Chim. Acta*, 2021, **515**, 120017, DOI: 10.1016/j.ica.2020.120017.

21 M. M. Rashad, A. M. Hassan, A. M. Nassar, N. M. Ibrahim and A. Mourtada, A new nano-structured Ni(II) Schiff base complex: synthesis, characterization, optical band gaps, and biological activity, *Appl. Phys. A*, 2014, **117**, 877–890, DOI: 10.1007/s00339-014-8448-6.

22 I. Warad, Y. Al-Demeri, M. Al-Nuri, S. Shahwan, M. Abdoh, S. Naveen, N. K. Lokanath, M. S. Mubarak, T. B. Hadda and Y. N. Mabkhot, Crystal structure, Hirshfeld surface, physicochemical, thermal and DFT studies of (N1E, N2E)-N1, N2-bis((5-bromothiophen-2-yl)methylene)ethane-1,2-diamine N2S2 ligand and its [CuBr(N2S2)]Br complex, *J. Mol. Struct.*, 2017, **1142**, 217–225, DOI: 10.1016/j.molstruc.2017.04.064.

23 J. V. Anguita, S. R. P. Silva, A. P. Burden, B. J. Sealy, S. Haq, M. Hebbron, I. Sturl and A. Pritchard, Thermal stability of plasma deposited thin films of hydrogenated carbon–nitrogen alloys, *J. Appl. Phys.*, 1999, **86**, 6276–6281.

24 A. S. Potapov, E. A. Nudnova, G. A. Domina, L. N. Kirpotina, M. T. Quinn, A. I. Khlebnikov and I. A. Schepetkin, Synthesis, characterization and potent superoxide dismutase-like activity of novel bis(pyrazole) – 2,2′-bipyridyl mixed ligand copper (II) complexes, *Dalton Trans.*, 2009, **23**, 4488–4498.

25 L. O. Onça, J. C. P. de Souza, I. G. N. dos Santos, E. d. S. Santos, S. M. Soares and P. H. G. D. Diniz, A new highly selective colorimetric Schiff base chemosensor for determining the copper content in artisanal cachaças, *Spectrochim. Acta, Part A*, 2020, **243**, 118783, DOI: 10.1016/j.saa.2020.118783.

26 A. Parween and S. Naskar, Synthesis and characterization of 1,2,4-triazole containing Schiff base ligands and their Cu II complexes, *J. Indian Chem. Soc.*, 2017, **94**, 135–140.

27 C. R. Lucas, S. Liu, M. J. Newlands, J.-P. Charland and E. J. Gabe, Thiophenophane metal complexes. II. Preparation, structure, and properties of binuclear copper(II) complexes and of 2,5,9,12-tetrathia[13](2,5)thiophenophane. Evidence for *S*-coordinated thiophene, *Can. J. Chem.*, 1989, **67**, 639–647, DOI: 10.1139/v89-096.

28 D. Lörchner, D. Dittmann, U. Braun, L. W. Kroh and R. Köppen, Investigation of two triazine-based heterocyclic brominated flame retardants by coupled thermogravimetry-Fourier transform infrared spectroscopy, *J. Anal. Appl. Pyrolysis*, 2019, **141**, 104635, DOI: 10.1016/j.jaap.2019.104635.

29 L. Ali, K. Sivaramakrishnan, M. S. Kuttiyathil, V. Chandrasekaran, O. H. Ahmed, M. Al-Harahsheh and M. Altarawneh, Prediction of Thermogravimetric Data in Bromine Captured from Brominated Flame Retardants (BFRs) in e-Waste Treatment using Machine Learning Approaches, *J. Chem. Inf. Model.*, 2023, **63**, 2305–2320, DOI: 10.1021/acs.jcim.3c00183.

30 H. Wu, Y. Shen, N. Harada, Q. An and K. Yoshikawa, Production of Pyrolysis Oil with Low Bromine and Antimony Contents from Plastic Material Containing Brominated Flame Retardants and Antimony Trioxide, *Energy Environ. Res.*, 2014, **4**, 105–118, DOI: 10.5539/eer.v4n3p105.

31 J. R. Zamian, A. E. Mauro, C. C. Nunes and E. T. de Almeida, Thermal decomposition and stability in a series of heterobimetallic carbonyl compounds of the type [Fe(CO)4(HgX)2] (X=Cl, Br, I), *Eclét. Quím.*, 2000, **25**, 89–95, DOI: 10.1590/S0100-46702000000100008.

32 S. Raha and M. Ahmaruzzaman, Facile fabrication of g-C3N4 supported Fe3O4 nanoparticles/ZnO nanorods: A superlative visible light responsive architecture for express degradation of pantoprazole, *Chem. Eng. J.*, 2020, **387**, 123766, DOI: 10.1016/j.cej.2019.123766.

33 J. Ahemed, J. Pasha, V. Rao D, R. Kore, R. Gade, Y. Bhongiri, P. Chetti and S. Pola, Synthesis of new Zn (II) complexes for photo decomposition of organic dye pollutants, industrial wastewater and photo-oxidation of methyl arenes under

34 visible-light, *J. Photochem. Photobiol., A*, 2021, **419**, 113455, DOI: 10.1016/j.jphotochem.2021.113455.

34 R. Vallavoju, R. Kore, P. Radhika, M. Subburu, M. Basude, P. Chetti and S. Pola, Degradation of organic pollutants in the presence of new Mn (II) complexes under ambient light or darkness conditions, *J. Photochem. Photobiol., A*, 2023, **442**, 114775, DOI: 10.1016/j.jphotochem.2023.114775.

35 V. Gadore, S. R. Mishra and M. Ahmaruzzaman, Bio-inspired sustainable synthesis of novel SnS2/biochar nanocomposite for adsorption coupled photodegradation of amoxicillin and congo red: Effects of reaction parameters, and water matrices, *J. Environ. Manage.*, 2023, **334**, 117496, DOI: 10.1016/j.jenvman.2023.117496.

36 I. Georgaki, E. Vasilaki and N. Katsarakis, A study on the degradation of carbamazepine and ibuprofen by TiO2 & ZnO photocatalysis upon UV/visible-light irradiation, *Am. J. Anal. Chem.*, 2014, **5**, 518–534, DOI: 10.4236/ajac.2014.58060.

37 N. Goswami, H. P. Gogoi and P. Barman, Sunlight mediated efficient degradation of pantoprazole drug using A novel Cu(II)-unsymmetrical Bis-Schiff base complex: Mechanism, degradation pathway and reusability, *Surf. Interfaces*, 2025, **67**, 106606, DOI: 10.1016/j.surfin.2025.106606.

38 S. R. Mishra, V. Gadore and M. Ahmaruzzaman, Development of high-performance bi-functional novel CdSnS2 atom clusters for adsorption of rose Bengal and AOP-assisted degradation of methylene blue, *Environ. Sci.: Water Res. Technol.*, 2023, **9**, 586–602, DOI: 10.1039/D2EW00654E.

39 Z. Z. Vasiljevic, M. P. Dojcinovic, J. D. Vujancevic, I. Jankovic-Castvan, M. Ognjanovic, N. B. Tadic, S. Stojadinovic, G. O. Brankovic and M. V. Nikolic, Photocatalytic degradation of methylene blue under natural sunlight using iron titanate nanoparticles prepared by a modified sol–gel method, *R. Soc. Open Sci.*, 2020, **7**, 200708, DOI: 10.1098/rsos.200708.

40 H. Jing, C. Wang, Y. Zhang, P. Wang and R. Li, Photocatalytic degradation of methylene blue in ZIF-8, *RSC Adv.*, 2014, **4**, 54454, DOI: 10.1039/c4ra08820d.

41 T. Araya, S. Quan, J. Man-ke, M. Wan-hong, D. Johnson and H. Ying-ping, Selective Photocatalytic Degradation of Organic Pollutants Using a Water-Insoluble Zn-Schiff Base Complex, *Water, Air, Soil Pollut.*, 2016, **227**, 284, DOI: 10.1007/s11270-016-2995-8.

42 H. Sadiq, H. Sadiq, A. Garcia-Garcia, L. I. I. Rodriguez, K. Batool, H. H. Sharif and M. Sharif, Preparation and photocatalytic degradation of methylene blue using a sulfanilic acid-functionalized NiO/GO ternary composite with electrochemical evaluation, *RSC Adv.*, 2025, **15**, 40984–40997, DOI: 10.1039/d5ra05508c.

43 D. Ş. Bahçeci, A. A. Kocaeren, N. Demir and B. Dalgiç, Anti-bacterial, anti-oxidant activities of polymer-based metal complexes and their catalyst effects in presence of H2O2, *Iran. Polym. J.*, 2024, **33**, 141–156, DOI: 10.1007/s13726-023-01249-7.

44 C. J. Dhanaraj and S. S. S. Raj, Synthesis, characterization, and biological studies of Schiff base metal complexes derived from 4-aminoantipyrine, acetamide and p-

phenylenediamine, *Inorg. Chem. Commun.*, 2020, **119**, 108087, DOI: 10.1016/j.inoche.2020.108087.

45 S. Brahmchari and A. P. Mishra, C(sp2)=N(sp2) Bond Formation via Acid-Catalyzed Condensation of Benzil and 2-Amino-4-chlorophenol: Exploring Structure and Biomedical Applications of Schiff Base Metal Complexes, *ChemistrySelect*, 2025, **10**, e03996, DOI: 10.1002/slct.202503996.

46 S. Nath, S. Mandal, P. Sow, A. Samadder, D. B. Cordes and N. C. Saha, Design, Synthesis, Spectroscopic and Structural Characterization of a New Pyrimidine Derived Schiff-base Ligand and its Co^{III}, Ni^{II} and Cu^{II} Complexes: Evaluation of their Photocatalytic and Antidiabetic Activities, *Chem. Afr.*, 2025, **8**, 4233–4257, DOI: 10.1007/s42250-025-01402-0.

47 H. Wang, X.-Y. Zhang, C.-F. Bi, Y.-H. Fan and X.-M. Meng, Synthesis, crystal structures and photocatalytic properties of Zn(II), Ni(II), Co(II) complexes with a symmetric open-chain N$_2$O$_4$-donor bis-Schiff base ligand, *Transition Met. Chem.*, 2015, **40**, 769–777, DOI: 10.1007/s11243-015-9975-5.

48 D. L. Puspitarum, N. I. Istiqomah, R. M. Tumbelaka, A. Kusumaatmaja, D. Oshima, T. Kato and E. Suharyadi, High performance of magnetically separable and recyclable photocatalyst of green-synthesized CoFe$_2$O$_4$/TiO$_2$ nanocomposites for degradation of methylene blue, *Adv. Nat. Sci.: Nanosci. Nanotechnol.*, 2022, **13**, 045003, DOI: 10.1088/2043-6262/ac996b.

49 P. V. Viet and H. N. Tran, Adsorption and photocatalytic degradation of methylene blue by titanium dioxide nanotubes at different pH conditions, *Adv. Nat. Sci.: Nanosci. Nanotechnol.*, 2019, **10**, 045011, DOI: 10.1088/2043-6254/ab5100.

50 P. T. L. Huong, N. V. Quang, N. T. Huyen, H. T. Huong, D. A. Tuan, M. T. Tran, Q. V. Tran, T. N. Bach, N. Tu and V.-D. Dao, Efficiency enhancement of photocatalytic activity under UV and visible light irradiation using ZnO/Fe$_3$O$_4$ heteronanostructures, *Sol. Energy*, 2023, **249**, 712–724, DOI: 10.1016/j.solener.2022.12.011.

51 N. N. Dao, M. D. Luu, N. C. Pham, T. D. Doan, T. H. C. Nguyen, Q. B. Nguyen and T. L. Duong, Low-temperature synthesis and investigations on photocatalytic activity of nanoparticles BiFeO3 for methylene blue and methylene orange degradation and some toxic organic compounds, *Adv. Nat. Sci.: Nanosci. Nanotechnol.*, 2016, **7**, 045003, DOI: 10.1088/2043-6262/7/4/045003.

52 A. Ranjbari, K. K. Adhikary, M. Kashif, A. P. Anbari, T. R. Siddhartha, D. Kim, S. Yoon, J. Yoon and P. M. Heynderickx, Comparative photocatalytic degradation of cationic rhodamine B and anionic bromocresol green using reduced ZnO: A detailed kinetic modeling approach, *Chemosphere*, 2025, **371**, 144052.

53 A. Machrouhi, H. Khiar, A. Elhalil, M. Sadiq, M. Abdennouri and N. Barka, Synthesis, characterization, and photocatalytic degradation of anionic dyes using a novel ZnO/activated carbon composite, *Watershed Ecol. Environ.*, 2023, **5**, 80–87.

54 Organització Mundial de la Salut, *Guidelines for Drinking-Water Quality: First Addendum to Third Edition. Recommendations*, World Health Organization, 2006.

55 A. Nandi and B. Chatterjee, Scavenging of superoxide radical by ascorbic acid, *J. Biosci.*, 1987, **11**, 435–441.

56 S.-A. Cheng, W.-K. Fung, K.-Y. Chan and P. K. Shen, Optimizing electron spin resonance detection of hydroxyl radical in water, *Chemosphere*, 2003, **52**, 1797–1805, DOI: 10.1016/S0045-6535(03)00369-2.

57 Z. Ma, B. Zhao and Z. Yuan, Application of electrochemical and spin trapping techniques in the investigation of hydroxyl radicals, *Anal. Chim. Acta*, 1999, **389**, 213–218, DOI: 10.1016/S0003-2670(99)00142-7.

58 Q.-Q. Xiao, Z.-W. Song, Y.-H. Li and G.-H. Cui, Two difunctional Co(II) coordination polymers for natural sunlight photocatalysis of methylene blue and selective fluorescence sensing of Cr(VI) ion in water media, *J. Solid State Chem.*, 2019, **276**, 331–338, DOI: 10.1016/j.jssc.2019.05.025.

59 G. Vishnu, S. Singh, T. S. S. K. Naik, R. Viswanath, P. C. Ramamurthy, P. Bhadrecha, H. S. B. Naik, J. Singh, N. A. Khan and S. Zahmatkesh, Photodegradation of methylene blue dye using light driven photocatalyst-green cobalt doped cadmium ferrite nanoparticles as antibacterial agents, *J. Cleaner Prod.*, 2023, **404**, 136977, DOI: 10.1016/j.jclepro.2023.136977.

60 S. Raha and M. Ahmaruzzaman, A novel Ag/g-C3N4/ZnO/Fe3O4 nanohybrid superparamagnetic photocatalyst for efficient degradation of emerging pharmaceutical contaminant (Pantoprazole) from aqueous sources, *J. Environ. Chem. Eng.*, 2022, **10**, 108904, DOI: 10.1016/j.jece.2022.108904.

61 M. A. Rauf, M. A. Meetani, A. Khaleel and A. Ahmed, Photocatalytic degradation of Methylene Blue using a mixed catalyst and product analysis by LC/MS, *Chem. Eng. J.*, 2010, **157**, 373–378, DOI: 10.1016/j.cej.2009.11.017.

62 X. Teng, J. Li, Z. Wang, Z. Wei, C. Chen, K. Du, C. Zhao, G. Yang and Y. Li, Performance and mechanism of methylene blue degradation by an electrochemical process, *RSC Adv.*, 2020, **10**, 24712, DOI: 10.1039/d0ra03963b.

63 M. A. Abu-Dalo, S. A. Al-Rosan and B. A. Albiss, Photocatalytic Degradation of Methylene Blue Using Polymeric Membranes Based on Cellulose Acetate Impregnated with ZnO Nanostructures, *Polymers*, 2021, **13**, 3451, DOI: 10.3390/polym13193451.